Journal of Materials Chemistry A

PAPER

View Article Online
View Journal | View Issue

Cite this: J. Mater. Chem. A, 2017, 5, 24361

Al_2O_3 surface coating on $LiCoO_2$ through a facile and scalable wet-chemical method towards high-energy cathode materials withstanding high cutoff voltages†

Aijun Zhou,[a] Qin Liu,[a] Yi Wang,[b] Weihang Wang,[a] Xu Yao,[a] Wentao Hu,[c] Long Zhang,[c] Xiqian Yu,*[b] Jingze Li*[a] and Hong Li[b]

Received 18th August 2017
Accepted 24th October 2017

DOI: 10.1039/c7ta07312g

rsc.li/materials-a

With the increasing demand for high energy density in portable-device Li-ion batteries (LIBs), efforts are devoted to increase and stabilize the capacity of $LiCoO_2$ at high operation voltages. Herein, we report a low-cost and eco-friendly wet-chemical method to coat Al_2O_3 on $LiCoO_2$, using only aluminium sulphate and water as source materials. A nanoscale oxide layer is coated on the surface of $LiCoO_2$ particles through hydrogen-bonding assisted adsorption of the hydrolysed $Al(OH)_3$ nanoparticles. The as-proposed Al_2O_3-coating provides excellent physico-chemical protection and kinetically-favourable interfaces for the $LiCoO_2$ electrode, resulting in remarkable improvements of the electrode's cycling stability and rate capability when tested at high cutoff voltages up to 4.7 V (*vs.* Li/Li^+). The synergetic effects of the oxide coating, *e.g.* alleviated electrolyte decomposition and reduced generation of irreversible solid electrolyte interphase (SEI) constituents (LiF/Li_2CO_3 and organics), are attributed to the improvements. At the cutoff voltage of 4.5 V, the modified $LiCoO_2$ electrode in this work exhibits excellent cycling stability (147 mA h g^{-1}, 82.6% retention after 500 cycles at 1C) and competitive rate capability (130 mA h g^{-1} at 10C), which are some of the best results reported so far. The outstanding high-voltage electrode performance and the simple and scalable coating approach show great promise of $LiCoO_2$ cathodes in future high-energy and high-power LIBs.

Introduction

The pursuit of high-performance electrode materials is a crucial task for scientists and engineers around the world to develop next-generation high-energy Li-ion batteries (LiBs).[1–4] Since the 1990s, $LiCoO_2$ has become the most prominent cathode material for commercial LiBs due to its high specific capacity, high voltage output, good cycling stability and easy fabrication.[5,6] Although its derivative oxides such as $LiNi_{1-x-y}Co_yAl_xO_2$ (NCA) and $LiNi_{1-x-y}Co_yMn_xO_2$ (NCM) have emerged as low-cost cathodes that may replace $LiCoO_2$ in the future,[7–9] $LiCoO_2$ is of no doubt dominating the cathode market for small-format LIBs adapted for high-end consumable electronics due to its much higher gravimetric energy density (W h L^{-1}) than others. This situation is expected to continue for quite a long time until essential progress can be made on other materials. Despite the long history of $LiCoO_2$, the research interest in fundamental studies and new applications of this material has never declined.[10–12] Driven by the demand for higher energy/power density of LIBs for the rising market of smart phones and tablets, battery industries and scientists are trying to elevate the charging voltage of $LiCoO_2$/graphite batteries above the conventional limit of 4.25–4.3 V.[13,14] It is known that the electrochemical performances of $LiCoO_2$ are inherently dependent on the charging cutoff potential or voltage (*vs.* Li/Li^+).[15,16] At higher voltages, it is possible to extract more Li^+ from the layered $LiCoO_2$ lattice and thus can increase the discharge capacity, energy density and the working voltage of the cells (Fig. S1†). Unfortunately, pristine $LiCoO_2$ suffers from a poor cycling stability at high voltages owing to structural or chemical degradations of both active materials and electrolyte,[17] imposing restrictions for its high-voltage applications.

[a]State Key Laboratory of Electronic Thin Films and Integrated Devices, School of Microelectronics and Solid-State Electronics, University of Electronic Science and Technology of China, Chengdu 610054, China. E-mail: lijingze@uestc.edu.cn; Fax: +86-28-83202569; Tel: +86-28-83207620

[b]Beijing National Laboratory for Condensed Matter Physics, Institute of Physics, Chinese Academy of Sciences, Beijing 100190, China. E-mail: xyu@iphy.ac.cn; Fax: +86-10-82649046; Tel: +86-10-82649413

[c]State Key Laboratory of Metastable Materials Science and Technology, Yanshan University, Qinhuangdao 066004, China

† Electronic supplementary information (ESI) available: Voltage dependences of capacity and energy density, EELS results, initial charge–discharge curves, coulombic efficiency data, effect of coating duration, long-term cycling stability, repeating experimental results, CV data, fitting results of surface layer resistance, FESEM images of cycled electrodes, and XPS analysis results. See DOI: 10.1039/c7ta07312g

In order to address the high-voltage issues of $LiCoO_2$, many strategies including doping,[18,19] surface coating[20–22] and electrolyte addition[23,24] have been employed. The major trend is toward surface modification by coating $LiCoO_2$ with a particular material in order to physically or/and chemically protect the active materials from electrolyte corrosion or enhance the solid/liquid interfaces. So far, there have been a large number of literature studies reporting the surface coating of $LiCoO_2$, among which the Al_2O_3 coating has attracted the greatest attention due to the most remarkable improvements in electrochemical performances.[19,25–33] Generally, it is believed that Al_2O_3 coating on $LiCoO_2$ is likely to result in the formation of $LiAlO_2$ or $LiAl_xCo_{1-x}O_2$ solid solution interphase layers which can passivate the electrode surface and enhance the interfacial kinetics.[13,34–36] Other mechanisms, such as scavenging detrimental HF generated from electrolyte decomposition, mitigating side reactions and irreversible growth of solid electrolyte interphase (SEI), and suppressing oxygen losses from the cathode, were also proposed to explain the effects of Al_2O_3 coating.[37–39]

The coating technologies for LIB materials can be generally categorized into two groups, namely solution-based (or wet-chemical) and vapour-based coatings. Typical approaches of the former group are sol–gel[40,41] and co-precipitation methods.[15,42,43] These wet-chemical treatments are usually followed by subsequent annealing of the as-obtained precursors. The latter group includes sputtering,[44,45] chemical vapour deposition (CVD),[46,47] atomic layer deposition (ALD),[48,49] *etc.*, which involve the deposition of coating materials in a closed vapour system. Note that in recent years the ALD-coating has received tremendous attention due to its self-limited ultra-thin (Å-level) and conformal coating, which has been proven effective for surface modification of many electrode materials.[27,50–52] However, from the industrial point of view, traditional wet-chemical coatings are more economic and easier to scale up than vapour-based coatings.

In most reports regarding Al_2O_3 wet-chemical coating, the coated materials were obtained by co-firing the chelated or precipitated $Al(OH)_3/LiCoO_2$ precursor mixture using an organic or inorganic Al-salt (*e.g.* $C_9H_{21}AlO_3$ or $Al(NO_3)_3$) as the source material.[35,41,53] Normally, a minimum level of 1 wt% Al_2O_3 addition was adopted, with little attention to possible self-precipitation of the oxide as an unnecessary secondary phase in the active materials. For precise control of the coating material, Zhang *et al.*[26] developed a novel organic buffer solution method which enabled nm-by-nm growth of Al_2O_3 on $LiCoO_2$ and on some other electrode materials. The cycling performance of the 1–2 nm-coated $LiCoO_2$ was improved at the cutoff voltage of 4.5 V. Despite these efforts, most literature only reported the cycling performances of $LiCoO_2$ within limited numbers of cycles (Table 1) under the high-voltage conditions, which makes it difficult to evaluate the practical long-term effect of the coatings. In addition, developing more simple, controllable and environmentally benign wet-chemical coating methods is also important to accelerate the application of high-voltage $LiCoO_2$, which is one of the central topics in the research community.

In this contribution, we report an extraordinarily simple but very effective way to coat Al_2O_3 on $LiCoO_2$, without the use of any chelate, precipitant (bases) or organic chemical. Only $Al_2(SO_4)_3$ aqueous solution is used in this work as the source material for coating *via* its time-dependent hydrolysis reaction and the strong adsorption of intermediate hydroxide products onto the $LiCoO_2$ surfaces. Instead of co-firing the overall mixture, the excess soluble cations and anions were washed away after the hydrolysis and adsorption process in order to avoid unnecessary precipitates of Al_2O_3 in the active materials. The electrochemical performances of the as-prepared $LiCoO_2$ were systematically investigated at high cutoff voltages from 4.5 V to 4.7 V with ultra-long cycling that has rarely been reported. At all cutoff voltages, the Al_2O_3-coated $LiCoO_2$ (AOLCO) electrodes show remarkable improvements in both cycling stability and rate capability as compared to the bare $LiCoO_2$ (BLCO) electrode. The long-term cycling performance of the Al_2O_3-coated $LiCoO_2$ at 4.5 V cutoff voltage is considered as one of the best results ever reported, while the coating process is facile and economic.

Experimental

Materials

$LiCoO_2$ powders (99.9%) were purchased from Hunan Changyuan Like Co., Ltd. Analytical grade $Al_2(SO_4)_3 \cdot 18H_2O$ was purchased from Chengdu Kelong Chemical Reagent Co. Ltd. All chemicals were used as received without further purification.

Wet-chemical coating

In a typical process, 0.135 g $Al_2(SO_4)_3 \cdot 18H_2O$ was dissolved in 50 mL deionized water, followed by adding 2.0 g $LiCoO_2$ powder which was dispersed by ultrasound for 30 min and vigorous stirring for 12 h at room temperature (RT). In this period, the hydrolysed $Al(OH)_3$ will adsorb on the surface of $LiCoO_2$ because of strong hydrogen bonding between the hydroxide and the oxide. After the adsorption process, careful centrifugation and washing were repeated several times in order to remove all remaining soluble ions. The obtained mixture was finally dried at 80 °C and calcined at 500 °C in air for 5 h, resulting in AOLCO powder. For a true comparison, the reference sample BLCO was obtained by treating the as-received $LiCoO_2$ powders with the same procedures above, only without adding $Al_2(SO_4)_3 \cdot 18H_2O$.

Electrode fabrication and cell assembly

The composite electrodes and the cells were fabricated following these procedures: first, BLCO or AOLCO active powders were thoroughly mixed with acetylene black (AB) and polyvinylidene fluoride (PVDF) with a weight ratio of 8 : 1 : 1 in *N*-methyl pyrrolidone (NMP). The obtained slurry was then homogeneously spread onto a piece of carbon-coated Al foil followed by vacuum-drying at 110 °C for 12 h. After that, the electrode foil was punched into discs of 10 mm in diameter for cell assembly. The selected electrodes with a loading density greater than 2 mg cm^{-2} were used for the assembly of $LiCoO_2$/Li half cells (CR2032-type), which was performed in an Ar-filled

Table 1 Overview of the high-voltage electrochemical performances of Al_2O_3-coated $LiCoO_2$ achieved by different methods

Coating type/material	Source material	Cutoff potentials (V *vs.* Li/Li^+)	Current density (1C = 140 mA g^{-1})	Max. cycle number	Max. capacity (mA h g^{-1})	Capacity retention	Ref.
Solution-Al_2O_3	$Al(NO_3)_3\cdot 9H_2O$	3.0–4.5	C/9	50	178	88.4%	29
	$Al(NO_3)_3\cdot 9H_2O$, $NH_3\cdot H_2O$	3.0–4.5	1.14C	70	170	96%	30
	$Al_2(SO_4)_3$, $HCOONH_4$, HCOOH	3.0–4.5	0.1C	50	172	93%	26
	$Al(NO_3)_3\cdot 9H_2O$, PVP, CH_3COOH or $NH_3\cdot H_2O$	3.0–4.5	0.5C	80	186	95%	31
	$Al(NO_3)_3\cdot 9H_2O$	3.7–4.5	0.1C	170	160	63%	33
	$Al_2(SO_4)_3$	3.0–4.5	1C	1000	178	72.5%	This work
ALD-Al_2O_3	$Al(CH_3)_3$	3.3–4.5	1C	30	175	99%	19
		3.3–4.5	0.71C	100	160	93.9%	27
		3.0–4.5	0.2C	50	190	79%	29
Sintering-Al_2O_3	Al_2O_3	3.7–4.5	0.1C	500	176	64%	32
Solution-AZO	$Al(NO_3)_3\cdot 9H_2O$, $Zn(CH_3COO)_2\cdot 2H_2O$, ethanol, MEA	2.75–4.5	0.71C	200	186	92.8%	41

glove-box, using 1 M $LiPF_6$ dissolved in ethylene carbonate (EC), diethyl carbonate (DEC) and dimethyl carbonate (DMC) (1 : 1 : 1, v/v, Shandong Hairong Power Supply Material Co., LTD.) as a liquid electrolyte. Prior to the cell assembly, the composite electrodes and separators (polypropylene, Celgard 2400) were dried overnight in a vacuum at 110 °C and 50 °C, respectively, in order to remove residual water.

Electrochemical tests

Galvanostatic charge/discharge tests of the cells were performed using a CT2001A cell test instrument (LAND Electronic Co.) from 3.0 V to different cutoff potentials (up to 4.7 V *vs.* Li/Li^+) at 1C (1C = 140 mA g^{-1}). The rate capability was tested stepwise from 0.02C to 10C. Cyclic voltammetry (CV) tests were carried out using Arbin BT2000 equipment with a sweep rate of 0.1 mV s^{-1}. Electrochemical impedance spectroscopy (EIS) measurements were performed using an electrochemical workstation (CHI660B) in the frequency range from 10^5 to 10^{-2} Hz with a perturbation voltage of 10 mV.

Material characterization

The phase of the materials was determined by X-ray diffraction (XRD, Dandong Haoyuan Instrument DX2700) using Cu Kα radiation (λ = 1.54056 Å). The microstructure was observed by using a field emission scanning electron microscope (FESEM, Hitachi S3400N) and a transmission electron microscope (TEM). The compositional information of the materials was analysed by using energy dispersive X-ray spectroscopy (EDS, Oxford INCA PentaFET-x3SDD) and electron energy loss spectroscopy (EELS). X-ray photoelectron spectroscopy (XPS, Thermo Fisher 250Xi) was used to analyse the surface of the powders and electrodes. For XPS measurements, Al-Kα (1486.6 eV) radiation was used as the primary excitation source (150 W), and the C 1s level (284.6 eV) was used as the internal reference for binding energy (BE). Ar^+ plasma etching was used to study the in-depth XPS information. The reference etching rate is 0.09 nm min^{-1} for Ta_2O_5.

Results and discussion

The material characterization results of the bare and coated $LiCoO_2$ powders are presented in Fig. 1 and 2. From the FESEM images (Fig. 1a–d) one can distinguish that the AOLCO grain is covered by an ambiguous substance, which can be observed more clearly from the TEM images (Fig. 2a and b). The thickness of the coating layer is estimated to be ~10 nm from the TEM image, and the electron diffraction (Fig. 2c and d) and XRD patterns (Fig. 1e) reveal basically the same hexagonal layered structure for the bare and coated $LiCoO_2$. Although the surface coating is morphologically observed and also compositionally evidenced by EDS and XPS, it cannot be detected by XRD due to its limited amount and poor crystallinity. As seen from the Al 2p spectra (Fig. 1g), the surface of AOLCO is rich in the Al–O bond.[54,55] The O 1s spectrum of AOLCO is also more complicated than that of BLCO. The lower-BE peak (529 eV) which exists in both samples can be attributed to the O–Co bonds of $LiCoO_2$.[54–56] However, in the higher BE region, the spectrum of AOLCO can be separated into two peaks which are contributed by O–Al bonds[54] and O–H bonds,[57] respectively. The latter is originated from hydroxyl groups adsorbed on the sample surface. All these results imply the successful oxide coating on $LiCoO_2$ powders by the as-proposed method. It was proposed that in Al_2O_3-coated $LiCoO_2$, the surface coating layer may be partially transformed into Li–Al–Co–O solid solutions through inter-diffusion of cations during the annealing process.[28,29,58] By closer observation of the XPS spectra, we can observe slight shifts of the Al and Co peaks in AOLCO as compared to those of BLCO. The energy position of the Al 2p peak (73.4 eV) is relatively lower than that of the peak of Al_2O_3 (75.8 eV),[19,54] but much closer to those of $LiAlO_2$ and $LiAl_{0.1}Co_{0.9}O_2$ (72.4 eV) reported by Appapillai *et al.*[55] In addition, the EELS measurement results (Fig. S2†) imply the existence of all elements (Li, Al, Co and O) in the surface coating layer part which proves the inter-diffusion phenomenon. Therefore, we believe that the surface of the AOLCO electrode contains a layer of Li–Al–Co–O solid solution, which was considered as a beneficial layer on $LiCoO_2$.

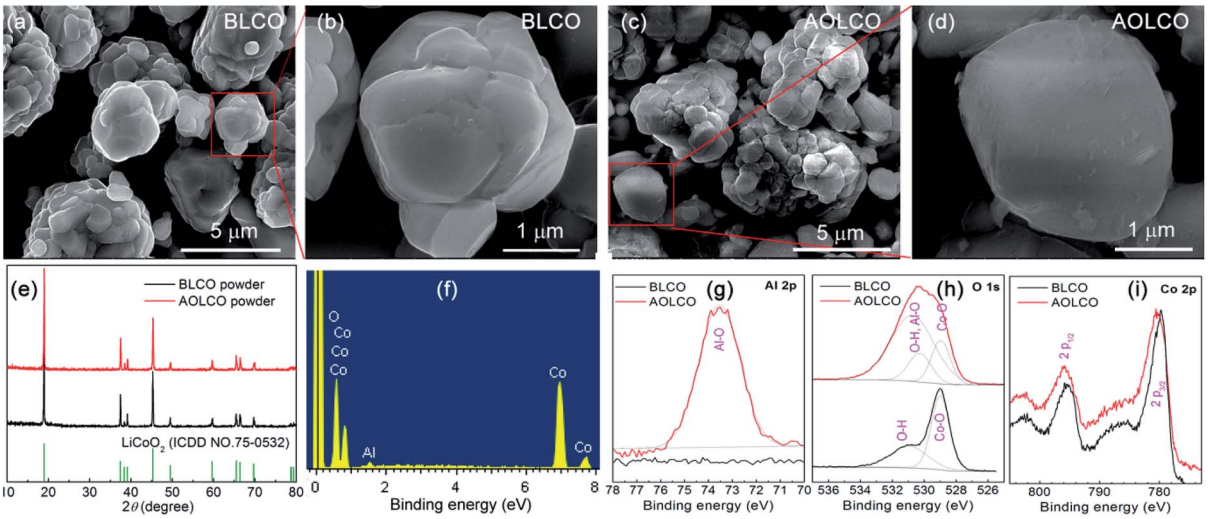

Fig. 1 Material characterization results of the bare and coated $LiCoO_2$ powders. (a–d) FESEM images, (e) XRD patterns, (f) EDS spectrum of AOLCO and (g–i) XPS spectra of both powders.

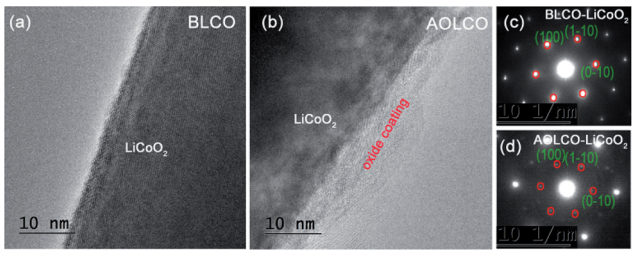

Fig. 2 (a and b) TEM images and (c and d) electron diffraction patterns of BLCO and AOLCO powders.

Recently, Han *et al.*[29] evidenced that the Li–Al–Co–O solid solution in Al_2O_3-coated $LiCoO_2$ starts to form at ~400 °C and the Al element will be completely doped into $LiCoO_2$ when the temperature reaches 800 °C. Considering the annealing temperature employed in this work (500 °C) is just above the formation temperature of the solid solution, we suppose that the surface coating layer on $LiCoO_2$ can be a two-phase constitutent comprising both the solid solution phase and some remaining Al_2O_3.

Fig. 3 shows the electrochemical performances of BLCO and AOLCO composite electrodes with the use of different cutoff voltages. It is evident that the initial capacity of the electrode can be increased by using higher cutoff voltages. However, such benefit is accompanied by poor cycling stability as seen in Fig. 3a. After a certain number of cycles, the bare electrode shows an abnormal decay in a catastrophic way indicating the fast propagation of irreversible side reactions which finally causes the termination of the cell. This phenomenon is found to occur in all BLCO/Li cells tested at different cutoff voltages. The lifespan of BLCO at 4.5 V cutoff is about 350 cycles, which is quickly reduced to 200 and 150 cycles as the cutoff voltage is increased to 4.6 V and 4.7 V, respectively. From the charge/discharge profiles (Fig. 3c–e), one can observe the fast increase of polarization in BLCO with increasing cutoff voltage or cycle number, resulting in a significant decrease of the discharge capacity. Taking the capacity value obtained at 4.2 V cutoff (prior to the high-voltage cycling) as a reference, which can represent the level of conventional $LiCoO_2$, the capacity improvement of BLCO after elevating the cutoff voltage will be completely offset after a short-term cycling (only 100 cycles). In contrast, the AOLCO electrode exhibits much better performances even at a high cutoff voltage of 4.7 V. The catastrophic failure as encountered in BLCO/Li cells is well suppressed by the wet-chemical Al_2O_3 coating as seen from the continuous operation of AOLCO/Li cells up to 500 cycles.

Although the AOLCO electrode shows relatively large early stage polarization than BLCO (*e.g.* at the initial cycle as shown in Fig. S3† and the 5th cycle as shown in Fig. 3c and d), which is due to the low electronic conductivity of Al_2O_3, the increase of the polarization during subsequent cycles can be effectively suppressed. In fact, we notice that the oxide coating is already effective at the very beginning of the cycling as reflected by the higher coulombic efficiency of AOLCO (Fig. S4†). At the cutoff voltage of 4.5 V, 4.6 V and 4.7 V, respectively, the AOLCO is able to deliver a capacity of 147, 96 and 52 mA h g^{-1} (83%, 45% and 24% retention) after 500 cycles, while the BLCO can only withstand such conditions for limited cycles after which the capacity decreases to zero. As a result, the AOLCO electrode can reach a higher energy density of 584, 361 and 167 W h kg^{-1} (based on the sole cathode) after 500 cycles at each cutoff voltage. Also note that the cycling stability of AOLCO can be affected by the duration of coating. Either too short or too long coating time can limit the improvements of the electrode and the coating time of 12 h is found to be an optimum value from our comparative results as shown in Fig. S5.†

The above results demonstrate that the performance of the $LiCoO_2$ electrode, even after coating, is highly sensitive to the cutoff voltage. The reduction of capacity, energy density and the average cell voltage during discharge (inset of Fig. 3b) becomes more and more significant when the cutoff is gradually

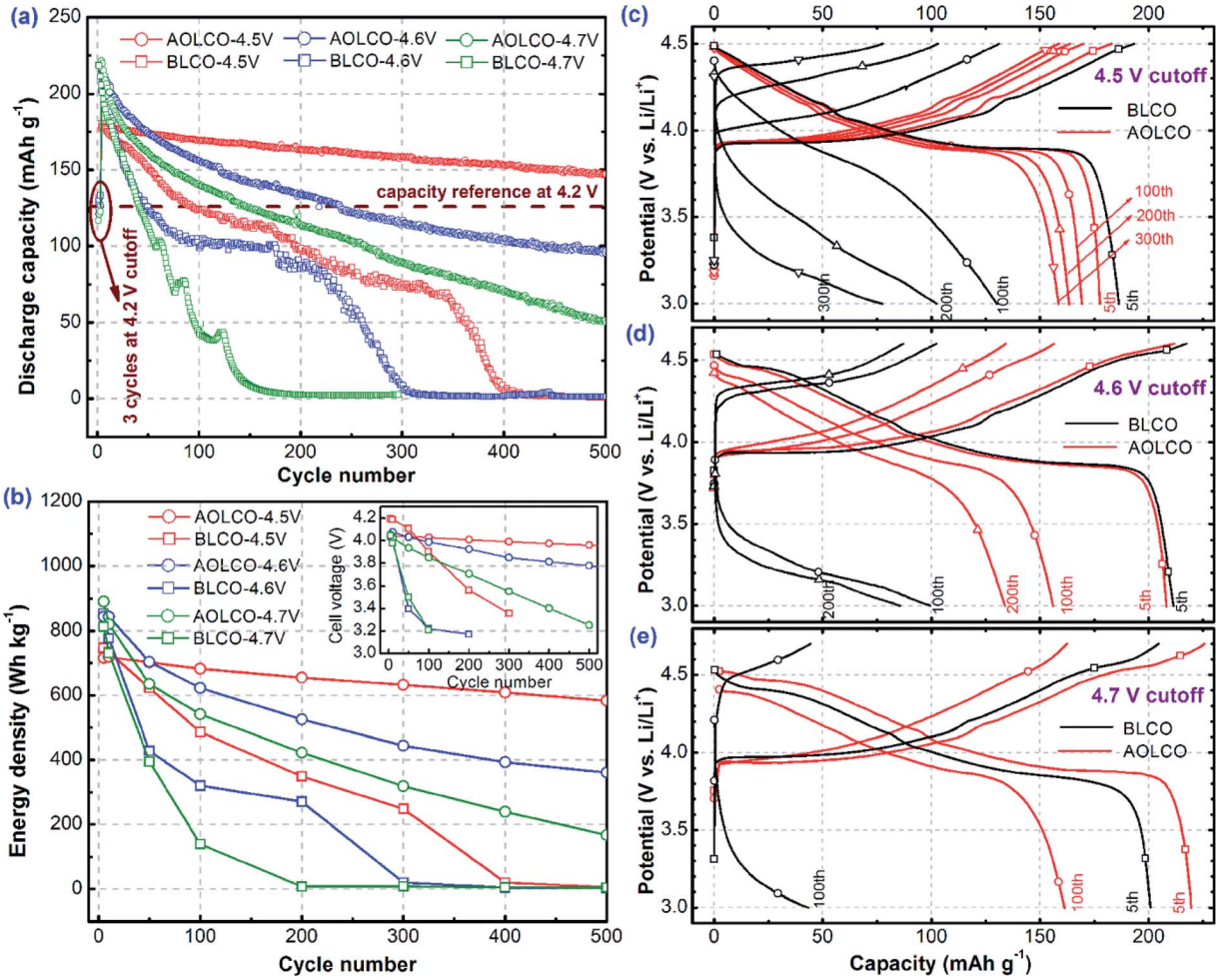

Fig. 3 Electrochemical performances of BLCO and AOLCO composite electrodes at different cutoff voltages from 4.5 V to 4.7 V at 1C and at RT. (a) Discharging capacity, (b) gravimetric energy density based on $LiCoO_2$ (the inset shows the average cell voltage calculated by dividing energy density by capacity) and (c–e) selected charge/discharge profiles at different cutoff voltages.

increased from 4.5 V to 4.7 V. Such behaviour was also observed in other related studies.[15,16] It is clear that applying 4.5 V cutoff yields the best cyclability for AOLCO. In fact, at this cutoff voltage, the as-modified electrode in this study is able to withstand even longer cycling over 1000 times (Fig. S6†), after which the remaining capacity can still reach 129 mA h g^{-1} (72.5% retention). Such outstanding performance of AOLCO is confirmed to be repeatable by duplicated experiments and measurements (Fig. S7†), suggesting good reliability of the as-proposed coating approach. At higher voltages (4.6 V and 4.7 V), however, although the Al_2O_3 coating can increase the lifespan of the electrode, the capacity and energy density of AOLCO at such voltages are not immune to fast degradation. The ultra-fast capacity decrease at 4.6 V and 4.7 V is partially caused by the reduced structural stability of $LiCoO_2$ due to the additional phase transformation as can be reflected by the CV curves (Fig. S8a–c†). On the other hand, decomposition of the liquid electrolyte (organic carbonates) is supposed to be more severe at such high voltages, which will be accompanied by complex chemical/electrochemical side reactions on the electrode surface.[59,60] The Al_2O_3 surface coating is found to be effective to tune the surface potential of the electrode (Fig. S8e and f†) and mitigate the side reactions on the interfaces.[35,36] However, it is not able to suppress the intrinsic structural collapse of $LiCoO_2$ and avoid electrolyte decomposition at higher voltages, which are responsible for the unfavourable long-term cyclability of AOLCO at 4.6 V and 4.7 V.

In addition to the cutoff voltage, the operation temperature is another key factor that strongly affects the performance of LIBs. As we know, self-heating is very common in LIBs and may cause serious performance degradation and even safety issues. Applying the optimal voltage of 4.5 V, the AOLCO electrode is further tested at 55 °C, which exhibits reduced cyclability as compared to its performance at RT (Fig. S6†). Nevertheless, the high-temperature performance of AOLCO is still better than that of the bare electrode at RT, showing a reversible capacity of 114 mA h g^{-1} after 500 cycles at 1C. This performance is very promising in the aspect of practical application.

The rate performances of electrodes at different cutoff voltages are compared in Fig. 4. At the current density of 10C, the

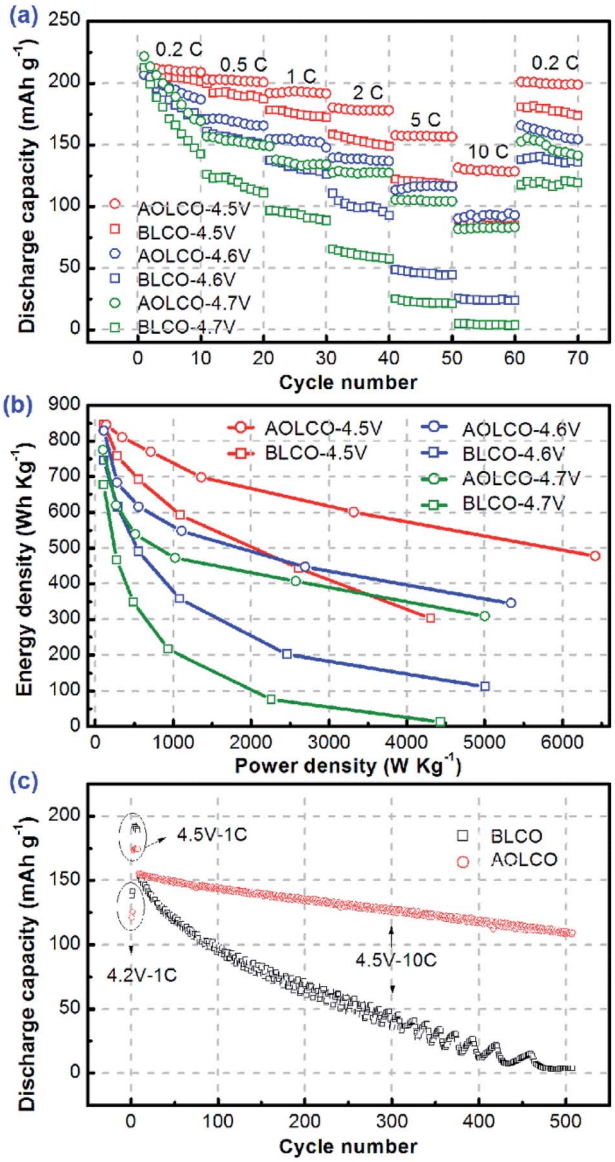

Fig. 4 (a) Rate performances of the BLCO and ALCO electrodes at different cutoff voltages at RT. (b) The relationship between energy density and powder density of the electrodes based on the rate performance data. (c) High-rate cycling stability of BLCO and AOLCO at 10C and 4.5 V cutoff voltage after a few formation cycles at a lower voltage and rate.

AOLCO electrode exhibits the largest reversible capacity of 130 mA h g^{-1} at 4.5 V, which is 54% greater than BLCO (84.5 mA h g^{-1}) (Fig. 4a). When returning to 0.2C after 50 cycles of transmission test, 95% of the initial capacity can be recovered for this electrode. Similar to the cycling performance, the rate capability at higher cutoff voltages (4.6 V and 4.7 V) is also very poor for the bare electrode, but still it can be considerably improved after the oxide coating. Fig. 4b plots the calculated energy density and power density based on the rate performance data. One can see that the Al_2O_3 coating not only can increase the energy density, but also leads to higher power density of $LiCoO_2$. At 10C and at the cutoff of 4.5 V, the improvement of power density is even more pronounced than the improvement of the energy density. For further validation of the electrode's high-rate performance at this voltage, the electrodes were cycled at 10C for a longer time. It is found that the AOLCO electrode has very promising high-rate cycling stability with over 70% capacity retention (109 mA h g^{-1}) after 500 cycles (Fig. 4c). In contrast, the capacity of BLCO has almost drained away after the same number of cycles. The superior high-rate performance of AOLCO at 4.5 V cutoff is encouraging because it provides the possibility of modified $LiCoO_2$ for use in future high-power and high-energy batteries.

In order to further understand the kinetics of the bare and coated electrodes, EIS measurements of the electrodes of different cycling depths and at different cut-off voltages were performed and the results are shown in Fig. 5. The Nyquist plots (Fig. 5a–d) are comprised of a liner part at low frequencies and two semicircles at high frequencies. The smaller semicircle represents the resistance of the surface layer (R_f), which has limited contribution to the total impedance and is found less dependent on the voltage and cycle number (Fig. S9†). The larger semicircle, representing charge transfer resistance (R_{ct}), is the major part of the impedance and reflects the kinetic properties of the interfaces including the $LiCoO_2$/SEI and SEI/electrolyte interfaces. It is found that the R_{ct} value and its increasing rate (with cycle number) is remarkably reduced after the oxide coating (Fig. 5e). The increased ratio of R_{ct} (100th/10th) is very large for BLCO, being ~630% and 930% at 4. 5 V and 4.6 V, respectively. Such a high increase of R_{ct} for BLCO suggests a quantitative increase or qualitative variation of the SEI formed on its surface during the long-term cycling. In contrast, the R_{ct} increase of AOLCO from the 10th to the 100th cycle is only 30% at the cutoff of 4.5 V. Although this ratio is further increased to 430% when the cutoff voltage is elevated to 4.6 V, it is still much smaller than that observed in BLCO. In addition, the analysis of the Warburg resistance (W, the linear part of the Nyquist plot) provides more information about the interfacial kinetics. As shown in Fig. 5f, the low frequency part of each Z'–$\omega^{1/2}$ plot can be well fitted to a straight line, the slope of which (k) is known to be inversely proportional to the diffusion coefficient of Li^+ (D_{Li^+}).[61] It is very evident that the k values of AOLCO are much smaller than those of BLCO after 100 cycles at both 4.5 V and 4.6 V, indicating much higher D_{Li^+} of AOLCO. These results clearly indicate that the transfer kinetics of Li^+ at the solid/liquid interfaces are significantly enhanced by the Al_2O_3 coating, which is responsible for the superior rate capability of AOLCO, especially at 4.5 V.

The observed differences in cycling stability and impedance increase for the bare and coated electrodes are supposed to be associated with their different morphological and compositional changes after electrochemical cycling. First, the grains of BLCO tend to crack easily after a certain period of cycling (Fig. S10a–c†) due to lattice expansion which generates more fresh interfaces and thus side reactions that favour a fast growth of SEI. However, with a nanoscale Al_2O_3 coating, which can be visually observed even after long-term cycling of AOLCO, the active materials are less likely to be disintegrated under the same cycling conditions (Fig. S10d–f†), which is important to maintain a more stable electrochemical performance. The

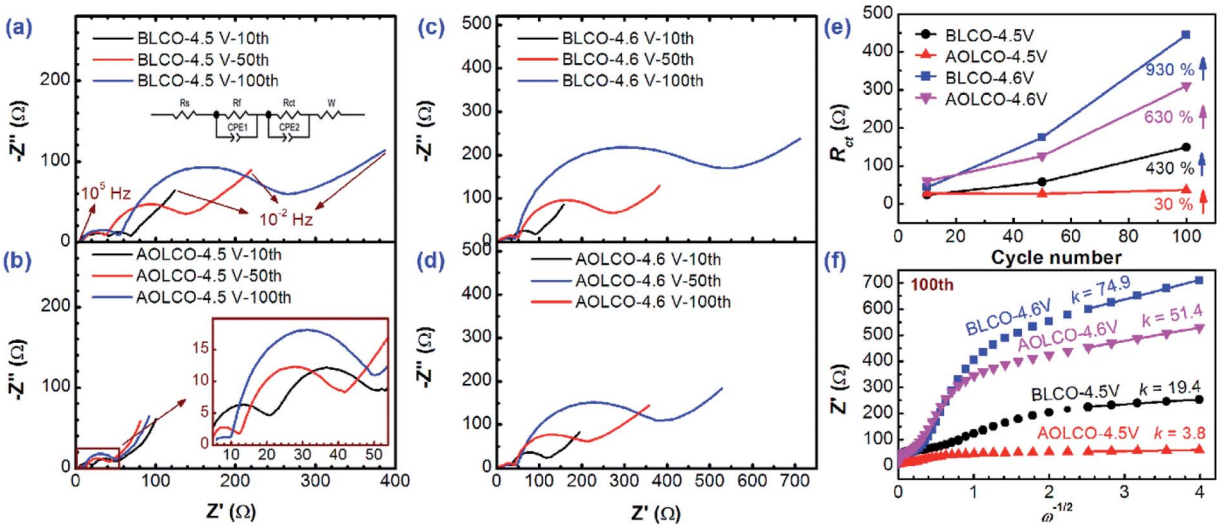

Fig. 5 (a–d) Nyquist plots of the BLCO and AOLCO electrodes after the 10th, 50th and 500th charge to different cutoff potentials. The insets in (a) and (c) show the equivalent circuit for data fitting and the zoom-in part of the Nyquist plots, respectively. (e) Fitted charge transfer resistances as a function of cycle number for BLCO and AOLCO electrodes cycled at the cutoff voltage of 4.5 V and 4.6 V. (f) Plots of the real part of impedance Z' as a function of $\omega^{-1/2}$, where ω is the angular frequency. The parameter k indicates the slope of the fitted lines.

compositional difference of the cycled electrodes could not be well distinguished through EDS because of the low sensitivity of EDS and the complexity of the cycled electrodes. For more clarification, XPS spectra were recorded for the electrodes before and after cycling at the cutoff voltage of 4.5 V which are summarized in Fig. 6. By comparison of these spectra, we can understand the effect of the Al_2O_3 coating on the generation of SEI on different electrodes. First of all, in the AOLCO electrode the intensity of Al 2p remains evident even after 500 cycles, suggesting that the oxide coating layer is chemically indissoluble in the electrolyte. The Co 2p peaks of this electrode after cycling (c-AOLCO) are also clearly observed after etching away the adsorbed substances such as electrolyte residuals remaining on the top surface. However, Co peaks cannot be observed

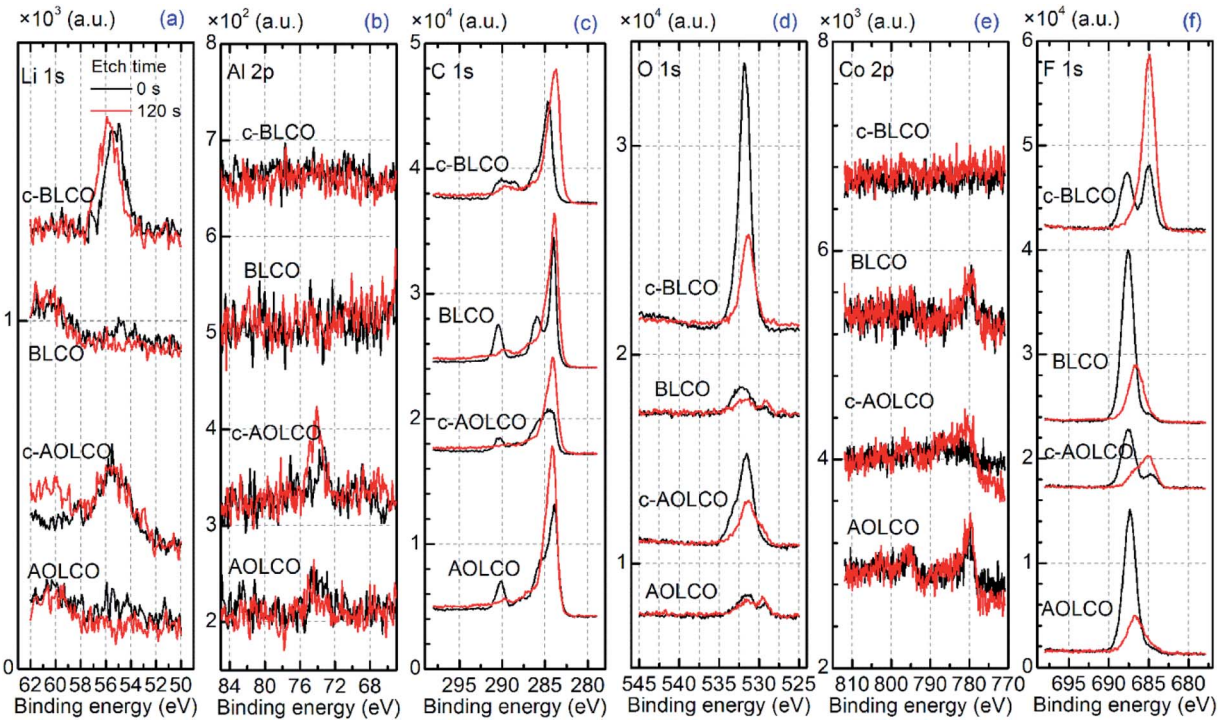

Fig. 6 XPS spectra of the BLCO and AOLCO electrodes before cycling and after 500 cycles of charge/discharge at the cutoff of 4.5 V (denoted by the letter "c"). (a) Li 1s, (b) Al 2p, (c) C 1s, (d) O 1s, (e) Co 2p and (f) F 1s. Note the different magnitudes in intensity.

on the cycled bare electrode (c-BLCO) even after the plasma etching. The Co-related secondary peaks in the O 1s and Li 1s spectra[62] are also distinguishable in c-AOLCO but absent in c-BLCO (Fig. S11a and b†). This comparison implies that the active materials on the surface of the electrode can be well preserved after high-voltage cycling due to the presence of Al_2O_3 coating, whereas they will easily react with electrolyte and be substituted by another substance if unprotected. Further analyses of the F 1s spectra reveal a large amount of LiF/Li_2CO_3 generation[63] on c-BLCO after 500 cycles at 4.5 V (Fig. S12c†). Such a trend is also observed at higher cutoff voltages (4.6 V and 4.7 V) after 200 cycles (Fig. S12†). LiF/Li_2CO_3 is known as one of the major chemical side reaction products in LIBs. Generally, it is believed that a small amount of these constituents (self-formed or intentionally coated) on electrode surfaces may be helpful for the electrochemical performance of LIBs because of the high chemical stability and ion-conducting nature.[37,64] However, since LiF and Li_2CO_3 are electronic insulators and their ionic conductivities are poorer than $LiCoO_2$, superfluous generation of LiF/Li_2CO_3 will lead to the fast increase of the electrode's overall impedance. Furthermore, as LiF and Li_2CO_3 are generally produced through electrolyte decomposition and acidic dissolution of $LiCoO_2$,[65] the uncontrolled *in situ* generation of LiF/Li_2CO_3 will continuously and irreversibly consume the active Li^+, which is one of the reasons causing capacity degradation. From the XPS analysis, it is found that the proportion of LiF in the F 1s spectra of c-AOLCO is much lower than that of c-BLCO at the cutoff of 4.5 V (Fig. S11c†). Besides, the SEI of c-AOLCO also contains less Li_2CO_3 and organic species than that of c-BLCO as suggested by the O 1s (Fig. S11a†) and C 1s spectra (Fig. S11d†).[56,63] These organic and inorganic constituents will grow irreversibly by sacrificing the electrolyte and active material, so the lifetime of the bare $LiCoO_2$ electrode at all studied cutoff voltages is limited. By the simple wet-chemical oxide coating, we believe that a more favourable SEI containing limited LiF/Li_2CO_3 and complex organics is formed under the high-voltage conditions with less electrolyte decomposition and interfacial side reactions, which should be responsible for the improvement of the electrode's high-voltage performances.

Table 1 lists a comparison of the state-of-the-art high-voltage capacities and retentions that have been achieved in $LiCoO_2$ after different surface coatings. Although different studies reported different capacity values, which could be in part due to the different pristine $LiCoO_2$ materials and different testing parameters (*e.g.* current density, cycle number and cutoff voltage) employed in each work, it is reasonable to compare the capacity retention values tested at the same charging cutoff voltage of 4.5 V. As shown in Fig. 7, the Al_2O_3-coated $LiCoO_2$ electrode in our work exhibits generally higher capacity retentions than other solution-coated electrodes. Our result is also comparable to the highest retention for $LiCoO_2$ at 4.5 V (92.8% retention after 200 cycles at ~0.7C) reported recently by Shen *et al.*[41] where $LiCoO_2$ was coated by Al-doped ZnO (AZO). In comparison with other coating methods, such as ALD coating, the capacity retention of our solution-coated $LiCoO_2$ is also among the best. For the first time, we demonstrate very promising and repeatable long-term cycling stability of 4.5 V-Al_2O_3-coated $LiCoO_2$ which can preserve 82.6/72.5% of its highest capacity after 500/1000 cycles and show excellent rate capability.

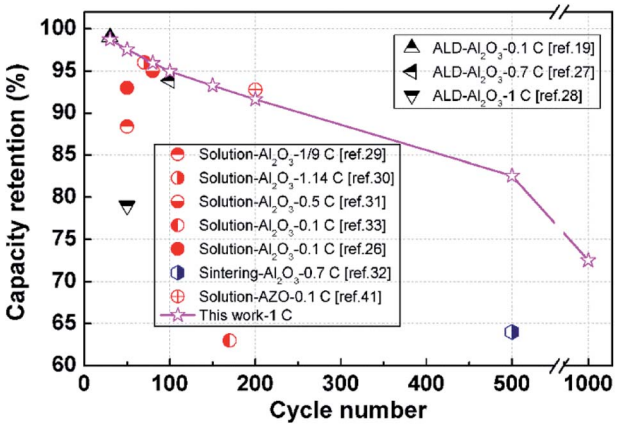

Fig. 7 Comparison of the cycling stability of surface-coated $LiCoO_2$ electrodes at the cutoff voltage of 4.5 V.

Conclusions

In summary, we report high-voltage (cutoff voltage from 4.5 V to 4.7 V) electrochemical performance $LiCoO_2$ modified by facile and scalable wet-chemical Al_2O_3 coating. The coated $LiCoO_2$ electrodes are most suitable for operation at 4.5 V cutoff voltage exhibiting a superior cycling stability and rate capability, while further increase of the cutoff voltage will lead to unacceptable cycling performances despite significant improvements as compared with the bare electrode. The Al_2O_3 coating is able to reduce the *in situ* production of LiF/Li_2CO_3 and organic species on the electrode surface, which are undesired SEI constituents in LIBs. Due to the high chemical stability of the oxide coating layer, the high-voltage induced electrolyte decomposition and irreversible side reactions are effectively mitigated. Meanwhile, the Li^+ diffusion through the solid–liquid interfaces is greatly enhanced. With over 70% capacity retention after long-term cycling for 1000 times (1C, 3.0–4.5 V) and an excellent high-rate performance (130 mA h g^{-1} at 10C), the as-proposed wet-chemical coating is testified as one of the most effective coatings for high-voltage $LiCoO_2$.

Conflicts of interest

There are no conflicts to declare.

Acknowledgements

This work is supported by the National Science Foundation of China (11234013, 21473022, 51502032, 21673033, and 51603028), Beijing Municipal Science & Technology Commission (D151100003115003), the Science and Technology Bureau of Sichuan Province of China (2017HH0089) and the

Fundamental Research Funds for the Central Universities of China (ZYGX2015J027).

Notes and references

1 J. B. Goodenough and Y. Kim, *Chem. Mater.*, 2010, **22**, 587–603.
2 F. Wang, S. Y. Song, J. Q. Li, J. Pan, X. Wang and H. J. Zhang, *Nanoscale*, 2017, **9**, 6346–6352.
3 L. L. Wu, Z. Wang, Y. Long, J. Li, Y. Liu, Q. S. Wang, X. Wang, S. Y. Song, X. G. Liu and H. J. Zhang, *Small*, 2017, **13**, 1604270.
4 Q. Zhu, Y. H. Li, Y. Gao, X. Wang and S. Y. Song, *Chem.–Eur. J.*, 2016, **22**, 6876–6880.
5 K. Mizushima, P. Jones, P. Wiseman and J. Goodenough, *Mater. Res. Bull.*, 1980, **15**, 783–789.
6 H. Li, Z. Wang, L. Chen and X. Huang, *Adv. Mater.*, 2009, **21**, 4593–4607.
7 N. Nitta, F. Wu, J. T. Lee and G. Yushin, *Mater. Today*, 2015, **18**, 252–264.
8 Y. Wang, J. Jiang and J. R. Dahn, *Electrochem. Commun.*, 2007, **9**, 2534–2540.
9 P. Zhou, H. Meng, Z. Zhang, C. Chen, Y. Lu, J. Cao, F. Cheng and J. Chen, *J. Mater. Chem. A*, 2017, **5**, 2724–2731.
10 Y. Xu, E. Hu, K. Zhang, X. Wang, V. Borzenets, Z. Sun, P. Pianetta, X. Yu, Y. Liu, X.-Q. Yang and H. Li, *ACS Energy Lett.*, 2017, **2**, 1240–1245.
11 Y. Gong, J. Zhang, L. Jiang, J.-A. Shi, Q. Zhang, Z. Yang, D. Zou, J. Wang, X. Yu, R. Xiao, Y.-S. Hu, L. Gu, H. Li and L. Chen, *J. Am. Chem. Soc.*, 2017, **139**, 4274–4277.
12 Y. Ito, S. Yamakawa, A. Hayashi and M. Tatsumisago, *J. Mater. Chem. A*, 2017, **5**, 10658–10668.
13 S. Kalluri, M. Yoon, M. Jo, S. Park, S. Myeong, J. Kim, S. X. Dou, Z. Guo and J. Cho, *Adv. Energy Mater.*, 2017, **7**, 1601507.
14 Y. Takahashi, S. Tode, A. Kinoshita, H. Fujimoto, I. Nakane and S. Fujitani, *J. Electrochem. Soc.*, 2008, **155**, A537–A541.
15 Z. Wang, C. Wu, L. Liu, F. Wu, L. Chen and X. Huang, *J. Electrochem. Soc.*, 2002, **149**, A466–A471.
16 A. M. Kannan, L. Rabenberg and A. Manthiram, *Electrochem. Solid-State Lett.*, 2003, **6**, A16–A18.
17 G. G. Amatucci, J. M. Tarascon and L. C. Klein, *Solid State Ionics*, 1996, **83**, 167–173.
18 S. Kim, S. Choi, K. Lee, G. J. Yang, S. S. Lee and Y. Kim, *Phys. Chem. Chem. Phys.*, 2017, **19**, 4104–4113.
19 M. Xie, T. Hu, L. Yang and Y. Zhou, *RSC Adv.*, 2016, **6**, 63250–63255.
20 K. T. Lee, S. Jeong and J. Cho, *Acc. Chem. Res.*, 2013, **46**, 1161–1170.
21 L. J. Fu, H. Liu, C. Li, Y. P. Wu, E. Rahm, R. Holze and H. Q. Wu, *Solid State Sci.*, 2006, **8**, 113–128.
22 S. Kalluri, M. Yoon, M. Jo, H. K. Liu, S. X. Dou, J. Cho and Z. Guo, *Adv. Mater.*, 2017, 1605807.
23 Y. Zhu, X. Luo, H. Zhi, X. Yang, L. Xing, Y. Liao, M. Xu and W. Li, *ACS Appl. Mater. Interfaces*, 2017, **9**, 12021–12034.
24 M. Zhou, C. Qin, Z. Liu, L. Feng, X. Su, Y. Chen, L. Xia, Y. Xia and Z. Liu, *Appl. Surf. Sci.*, 2017, **403**, 260–266.
25 N. V. Kosova and E. T. Devyatkina, *J. Power Sources*, 2007, **174**, 959–964.
26 W. Zhang, Z.-X. Chi, W.-X. Mao, R.-W. Lv, A.-M. Cao and L.-J. Wan, *Angew. Chem., Int. Ed.*, 2014, **53**, 12776–12780.
27 X. Li, J. Liu, X. Meng, Y. Tang, M. N. Banis, J. Yang, Y. Hu, R. Li, M. Cai and X. Sun, *J. Power Sources*, 2014, **247**, 57–69.
28 H.-M. Cheng, F.-M. Wang, J. P. Chu, R. Santhanam, J. Rick and S.-C. Lo, *J. Phys. Chem. C*, 2012, **116**, 7629–7637.
29 B. Han, T. Paulauskas, B. Key, C. Peebles, J. S. Park, R. F. Klie, J. T. Vaughey and F. Dogan, *ACS Appl. Mater. Interfaces*, 2017, **9**, 14769–14778.
30 D. D. Liang, H. F. Xiang, X. Liang, S. Cheng and C. H. Chen, *RSC Adv.*, 2017, **7**, 6809–6817.
31 D. Zuo, G. Tian, D. Chen, H. Shen, C. Lv, K. Shu and Y. Zhou, *Electrochim. Acta*, 2015, **178**, 447–457.
32 S. Sheng, G. Chen, B. Hu, R. Yang and Y. Xu, *J. Electroanal. Chem.*, 2017, **795**, 59–67.
33 G. Chen, H. Geng, Z. Wang, R. Yang and Y. Xu, *Ionics*, 2016, **22**, 629–636.
34 Z. Wang, *Solid State Ionics*, 2004, **175**, 239–242.
35 J. Cho, Y. J. Kim and B. Park, *Chem. Mater.*, 2000, **12**, 3788–3791.
36 Y. J. Kim, T. J. Kim, J. W. Shin, B. Park and J. P. Cho, *J. Electrochem. Soc.*, 2002, **149**, A1337–A1341.
37 M. Aykol, S. Kirklin and C. Wolverton, *Adv. Energy Mater.*, 2014, **4**, 1400690.
38 E. Jung and Y. J. Park, *J. Electroceram.*, 2012, **29**, 23–28.
39 P. Arora, R. E. White and M. Doyle, *J. Electrochem. Soc.*, 1998, **145**, 3647–3667.
40 G.-R. Hu, J.-C. Cao, Z.-D. Peng, Y.-B. Cao and K. Du, *Electrochim. Acta*, 2014, **149**, 49–55.
41 B. Shen, P. Zuo, Q. Li, X. He, G. Yin, Y. Ma, X. Cheng, C. Du and Y. Gao, *Electrochim. Acta*, 2017, **224**, 96–104.
42 A. Aboulaich, K. Ouzaouit, H. Faqir, A. Kaddami, I. Benzakour and I. Akalay, *Mater. Res. Bull.*, 2016, **73**, 362–368.
43 J. Cho, C. S. Kim and S. I. Yoo, *Electrochem. Solid-State Lett.*, 2000, **3**, 362–365.
44 X. Dai, A. Zhou, J. Xu, B. Yang, L. Wang and J. Li, *J. Power Sources*, 2015, **298**, 114–122.
45 X. Dai, L. Wang, J. Xu, Y. Wang, A. Zhou and J. Li, *ACS Appl. Mater. Interfaces*, 2014, **6**, 15853–15859.
46 W. Chang, J.-W. Choi, J.-C. Im and J. K. Lee, *J. Power Sources*, 2010, **195**, 320–326.
47 X. Wang and G. Yushin, *Energy Environ. Sci.*, 2015, **8**, 1889–1904.
48 S. M. George, *Chem. Rev.*, 2010, **110**, 111–131.
49 X. Meng, *J. Mater. Chem. A*, 2017, **5**, 10127–10149.
50 B. Ahmed, C. Xia and H. N. Alshareef, *Nano Today*, 2016, **11**, 250–271.
51 J. Liu and X. Sun, *Nanotechnology*, 2015, **26**, 024001.
52 X. Meng, X.-Q. Yang and X. Sun, *Adv. Mater.*, 2012, **24**, 3589–3615.
53 S. Amaresh, K. Karthikeyan, K. J. Kim, K. S. Nahm and Y. S. Lee, *RSC Adv.*, 2014, **4**, 23107–23115.
54 S. Verdier, L. El Ouatani, R. Dedryvere, F. Bonhomme, P. Biensan and D. Gonbeau, *J. Electrochem. Soc.*, 2007, **154**, A1088–A1099.

55 A. T. Appapillai, A. N. Mansour, J. Cho and Y. Shao-Horn, *Chem. Mater.*, 2007, **19**, 5748–5757.
56 E. Castel, E. J. Berg, M. El Kazzi, P. Novák and C. Villevieille, *Chem. Mater.*, 2014, **26**, 5051–5057.
57 E. McCafferty and J. P. Wightman, *Surf. Interface Anal.*, 1998, **26**, 549–564.
58 Y. Zhao, J. Li and J. R. Dahn, *Chem. Mater.*, 2017, **29**, 5239–5248.
59 A. Zhou, Y. Lu, Q. Wang, J. Xu, W. Wang, X. Dai and J. Li, *J. Power Sources*, 2017, **346**, 24–30.
60 A. Yano, M. Shikano, A. Ueda, H. Sakaebe and Z. Ogumi, *J. Electrochem. Soc.*, 2017, **164**, A6116–A6122.
61 C. Ho, I. D. Raistrick and R. A. Huggins, *J. Electrochem. Soc.*, 1980, **127**, 343–350.
62 L. Daheron, R. Dedryvere, H. Martinez, M. Menetrier, C. Denage, C. Delmas and D. Gonbeau, *Chem. Mater.*, 2008, **20**, 583–590.
63 Y.-C. Lu, A. N. Mansour, N. Yabuuchi and Y. Shao-Horn, *Chem. Mater.*, 2009, **21**, 4408–4424.
64 S. J. Shi, J. P. Tu, Y. Y. Tang, Y. Q. Zhang, X. Y. Liu, X. L. Wang and C. D. Gu, *J. Power Sources*, 2013, **225**, 338–346.
65 M. Balasubramanian, H. S. Lee, X. Sun, X. Q. Yang, A. R. Moodenbaugh, J. McBreen, D. A. Fischer and Z. Fu, *Electrochem. Solid-State Lett.*, 2002, **5**, A22–A25.